Smart Mater. Struct. 5 (1996) 121–128. Printed in the UK

Missile flight control using active flexspar actuators

Ron Barrett, R Steven Gross and Fred Brozoski

Auburn University, Aerospace Engineering Department, 211 Aerospace Engineering Building, Auburn, AL 36849-5338, USA

Received 10 July 1995, accepted for publication 13 November 1995

Abstract. A new type of subsonic missile flight control surface using piezoelectric flexspar actuators is presented. The flexspar design uses an aerodynamic shell which is pivoted at the quarter-chord about a graphite main spar. The shell is pitched up and down by a piezoelectric bender element which is rigidly attached to a base mount and allowed to rotate freely at the tip. The element curvature, shell pitch deflection and torsional stiffness are modeled using laminated plate theory. A one-third scale TOW 2B missile model was used as a demonstration platform. A static wing of the missile was replaced with an active flexspar wing. The 1 in $\times$ 2.7 in active flight control surface was powered by a bimorph bender with 5 mil PZT-5H sheets. Bench and wind tunnel testing showed good correlation between theory and experiment and static pitch deflections in excess of $\pm 14°$. A natural frequency of 78.5 rad s^{-1} with a break frequency of 157 rad s^{-1} was measured. Wind tunnel tests revealed no flutter or divergence tendencies. Maximum changes in lift coefficient were measured at $\Delta C_L = \pm 0.73$ which indicates that terminal and initial missile load factors may be increased by approximately 3.1 and 12.6 g respectively, leading to a greatly reduced turn radius of only 2400 ft.

1. Introduction

Active flight control has been explored by numerous technologists. One of the earliest investigations was conducted by Crawley and coworkers who constructed a bending–twist coupled graphite–epoxy plate which used conventionally attached piezoceramic sheets. When the plate was exposed to air-loads, it bent further, which increased the twist [1]. Since these early investigations, many others have examined active plates, rotor blades and airplane wings. Several of these investigations have been centered around flight control devices which may be used for nearly all types of aircraft. One of the more noteworthy was presented by Spangler and Hall who constructed an active, hinged flap powered by a bimorph piezoceramic beam [2]. They successfully demonstrated that large control surface deflections were possible in the low-subsonic flight regime. This was one of the first investigations to show deflections of a significant magnitude for flight control. Recent improvements in flexure design have demonstrated even greater deflection magnitudes [3]. After this early invention, a host of technologists confirmed the findings and began integrating active flaps and helicopter rotors including Samak and Chopra, who built a helicopter rotor with a trailing-edge flap actuator [4]. Griffin and Hanagud examined flaps with flexural hinges [5]. Giurgiutiu and coworkers studied the many different types of rotorcraft vibration control technique and drew conclusions on general feasibility [6].

One area of active flight control which has been investigated for the past 4 years has involved low-aspect-ratio surfaces which are specifically tailored for missiles. One of the earliest feasible designs used directionally attached piezoelectric (DAP) torque plates to pitch subsonic missile fin shells [7–12]. Pitch deflections of up to $\pm 4.5°$ were demonstrated on very low-aspect-ratio subsonic fins. Such torque-plate technology was directly related to efforts in the area of twist–active helicopter rotor blades such as those pursued by Chen and Chopra [13]. Unlike the rotorcraft investigations, however, low-aspect-ratio flight control surfaces could not be effectively *twisted* for flight control. Only *pitch* deflections of the entire surface proved suitable for flight control. Further examination of the torque-plate missile fins led to the free-spar torque-plate design which decouples the main spar and the torque-plate. This allows for higher pitch deflections and Mach numbers up to 0.7 [14, 15].

Because these investigations used torque-plates, a finite limit on pitch deflections was reached for small-scale prototype fins. This pitch deflection limit was directly related to the availability of extremely thin piezoelectric actuator material (under 2 mil thickness) and the significant percentage of work done by the DAP elements on the substrate in torsion. Accordingly, a new method of generating higher pitch deflections of small-scale fins was sought. This paper deals with one approach to producing very high pitch deflections with a very simple type of piezoceramic actuator element. Using this new

0964-1726/96/020121+08$19.50

'flexspar' configuration, several unmanned aerial vehicles using piezoceramic flexspars for flight control have been built and flown [16]. Accordingly, the major goal of this study is to further investigate this new type of flight control device and demonstrate its performance on a scaled subsonic missile.

2. Actuator modeling

2.1. Bender element modeling

The actuator employed by the flexspar flight control surface is extremely simple and has been successfully modeled by numerous technologists. Using the techniques outlined by Jones, an estimation of actuator element curvature can be obtained [17]

$$\begin{Bmatrix} N \\ M \end{Bmatrix}_{ex} + \begin{Bmatrix} N \\ M \end{Bmatrix}_{a} + \begin{Bmatrix} N \\ M \end{Bmatrix}_{t} = \begin{bmatrix} A & B \\ B & D \end{bmatrix}_{l} \begin{Bmatrix} \varepsilon \\ \kappa \end{Bmatrix}_{l} \tag{1}$$

Assuming no externally applied forces are present on the element, only piezoelectric and thermally induced strains will generate extensions and curvatures which are equal in both directions. Equation (1) may be expanded to show the thermally induced strain and piezoelectric strain terms. Equation (2) assumes that the actuator element is completely isotropic and generates in-plane strains which are equal in all directions. (Actual piezoceramic actuators generate slightly different strains through the difference in d_{31} and d_{32} and have different stiffnesses through inherent orthotropy and shear-lag induced directional attachment.)

$$\begin{aligned} &\begin{bmatrix} A_{11}+A_{12} & 0 \\ 0 & D_{11}+D_{12} \end{bmatrix}_{lam} \begin{Bmatrix} \varepsilon \\ \kappa \end{Bmatrix} \\ &= \begin{bmatrix} A_{11}+A_{12} & 0 \\ 0 & D_{11}+D_{12} \end{bmatrix}_{a} \begin{Bmatrix} \alpha\Delta T \\ 0 \end{Bmatrix}_{a} \\ &\quad + \begin{bmatrix} A_{11}+A_{12} & 0 \\ 0 & D_{11}+D_{12} \end{bmatrix}_{s} \begin{Bmatrix} \alpha\Delta T \\ 0 \end{Bmatrix}_{s} \\ &\quad + \begin{bmatrix} 0 & B_{11}+B_{12} \\ B_{11}+B_{12} & 0 \end{bmatrix}_{a} \begin{Bmatrix} \Lambda \\ 0 \end{Bmatrix} \end{aligned} \tag{2}$$

Equation (2) is arranged assuming the actuator elements are energized in opposite directions so as to induce a bending curvature. If they were energized in the same direction, then the cross-coupling 'B' terms would go to zero and axial and bending terms would show up in the matrix. Assuming that a finite bond thickness, t_b, is present between the substrate (s) and the actuator (a) the laminate curvature, κ, follows from equation (2).

$$\kappa = \frac{E_a\left(t_s t_a + 2t_b t_a + t_a^2\right)\Lambda}{E_s t_s^3/12 + E_a\left((t_s+2t_b)^2 t_a/2 + (t_s+2t_b)\,t_a^2 + \frac{2}{3}t_a^3\right)} \tag{3}$$

It is assumed in equation (3) that the bond material has a negligible stiffness and that no shear lag is present in the laminate.

Another simple estimation for the amount of thermally induced strain in the laminate may be obtained by expanding equation (2) as shown below.

$$\varepsilon = \frac{2E_a t_a \alpha_a\,\Delta T + E_s t_s \alpha_s\,\Delta T}{2E_a t_a + E_s t_s} \tag{4}$$

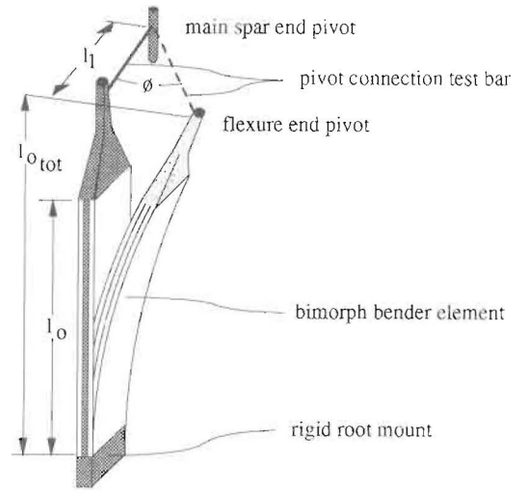

Figure 1. The geometry of a flexspar actuator with an active bender element.

Equation (4) is used to approximate the amount of prestress an actuator element is experiencing due to thermal effects. This is especially important as many piezoceramics have very low strains to failure in tension and should be precompressed by an elevated-temperature cure.

2.2. Flexspar actuator modeling

The flexspar actuator uses a bender element which may be analyzed by the procedures of 2.1. The result of this analysis is to relate actuator curvature, κ, and induced strain, Λ. This section will further extend the analysis to relate κ to pitch deflection of the wing surface. The actuator geometry which is used in the most common form of flexspar actuator is shown in figure 1.

In addition to the configuration shown a number of different actuator arrangements have been designed, tested and flown [16]. Results have shown that the deflection and stiffness vary most strongly with bender properties, l_0, $l_{0_{tot}}$ and l_1. An estimation of the rotational deflection of the actuator may be obtained by assuming that the flexure end pivot is allowed to slide freely along so that the pivot connection bar always makes contact at a distance $l_{0_{tot}}$ from the root mount. Equation (5) shows the pitch deflection as a function of geometry and bender element curvature:

$$\phi = 2\sin^{-1}\left[\frac{(1/\kappa)(1-\cos(\kappa l_0)) + (l_{0_{tot}} - (1/\kappa)\sin(\kappa l_0))\sin(\kappa l_0}{2l_1}\right] \tag{5}$$

This estimation does not account for any geometric stiffening effects due to rotational or extensional constraint. On experimental models, these geometric constraints have been shown to be small up to ±15° pitch deflection.

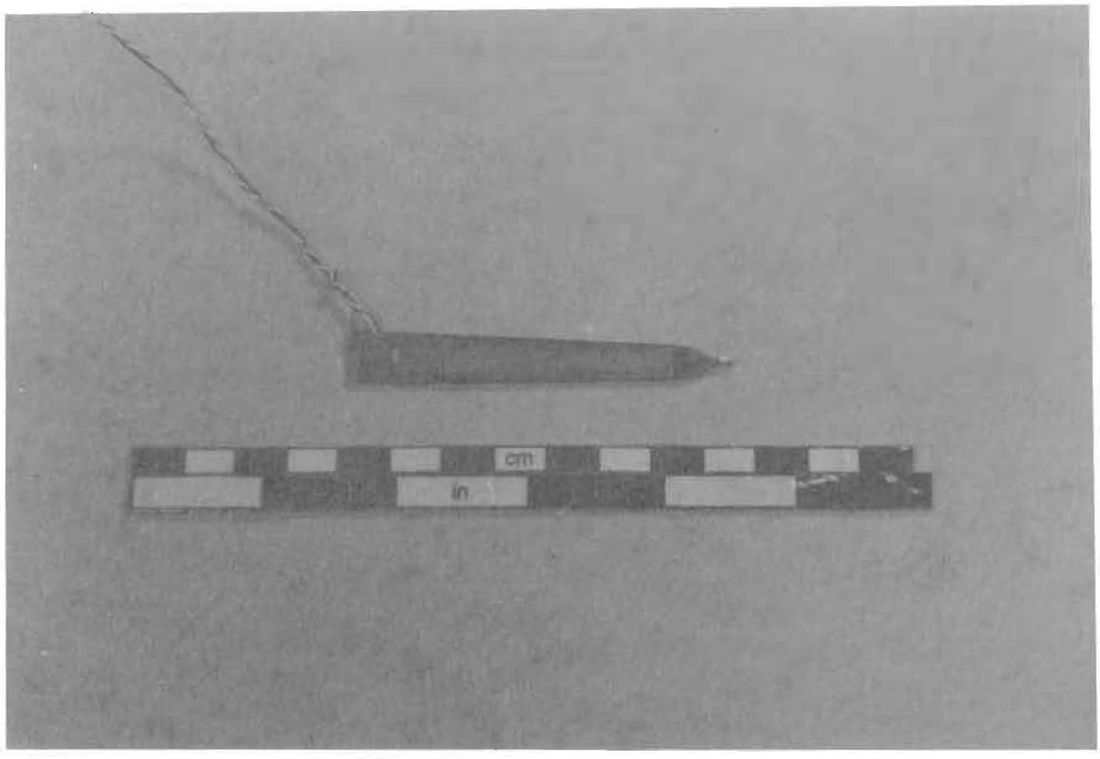

Figure 2. A bimorph bender element with a root mount and an end pivot.

Table 1. Piezoceramic bender element material properties.

	E (msi)	t (mil)	α (μstrain °F^{-1})	ϵ prestress
Substrate	14.5	3	9.8	1089 μstrain tension
Bond	< 1	2.5	—	—
PZT-5H	8.85	5	4	535 μstrain compression

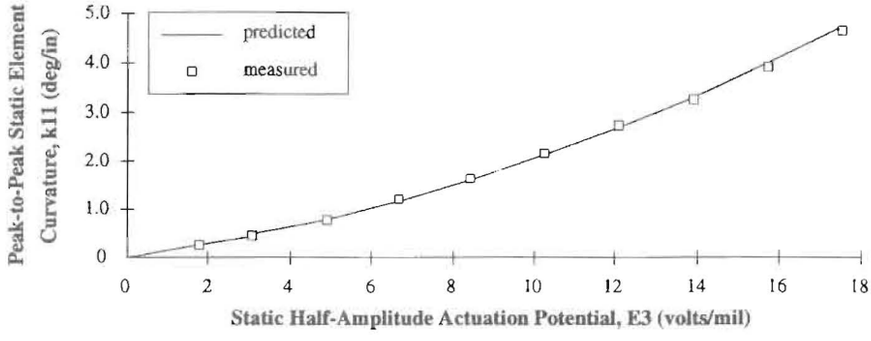

Figure 3. Static bender element curvature as a function of actuation potential.

3. Actuator construction and testing

3.1. Bender element fabrication

The first component of the experimental specimen to be constructed was the bender element. This element was formed with two sheets of 5 mil thick PZT-5H piezoceramic material which were laminated on to a 3 mil thick brass foil. The first step of fabrication involved wet cutting the elements to 2.5 in length × 0.4 in width at the base and 0.3 in width at the tip. After the elements had been cut, the substrate was trimmed to a similar size and the elements were joined to the substrate with Scotchweld™ adhesive tape and cured at 350 °F under 8 psi of pressure. After curing, the elements were deflashed, leads were attached to the substrate and faces and a section of style 120 fiberglass

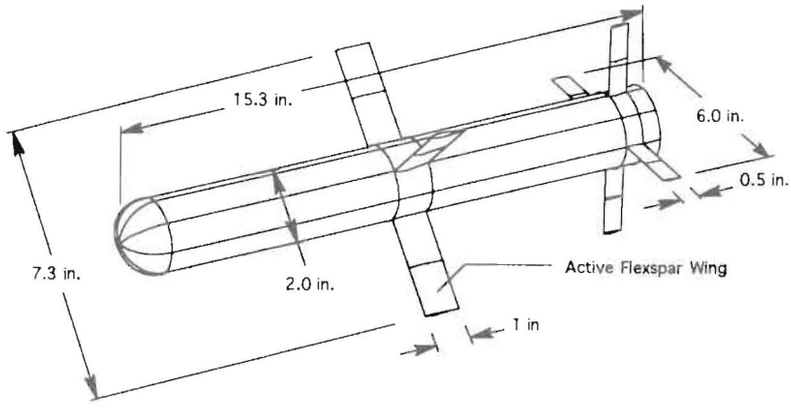

Figure 4. The scaled TOW 2B model geometry.

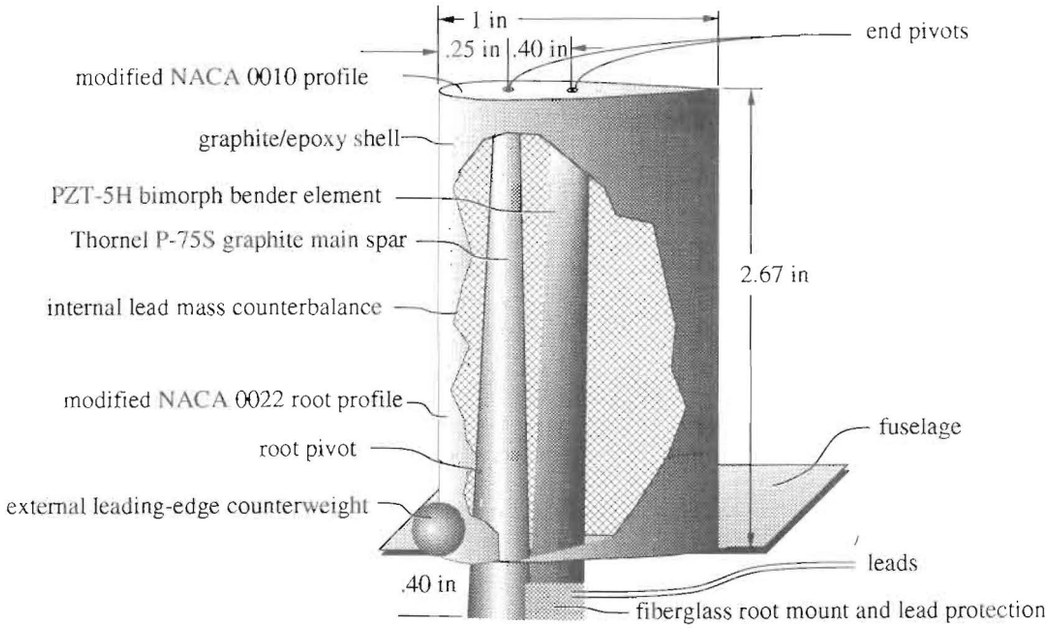

Figure 5. The flexspar missile wing internal structure.

Table 2. Piezoceramic bender element material properties.

	Maximum peak-to-peak pitch deflection ϕ (°) ($\Lambda = \pm 220$ μstrain)	Natural frequency (Hz)	Weight (oz)	Maximum RMS power consumption (mW)
Actuator prediction	± 17.1	61	0.19	< 10
Actuator actual	± 16.25	55	0.22	< 10
Wing prediction	± 17.1	16	0.35	< 10
Wing test	± 14.1	12	0.448	< 10
Full-scale wing (est.)	± 16	8	12.1	< 470

root stiffener was added to the element base to provide protection for the leads and a structurally strong attachment point. The end of the flexure element was modified with an end pivot which was also attached with style 120 fiberglass. The geometry of the bender element is shown in figure 2.

Because the bender element was cured at an elevated temperature, the PZT elements were prestressed in compression. This was done to ensure that the elements would not experience tensile stresses during normal operation, which often leads to breakage or defacing. Using equation (4), test data and manufacturers' data, the amount of precompression along with several other important characteristics of the bender will determined [18].

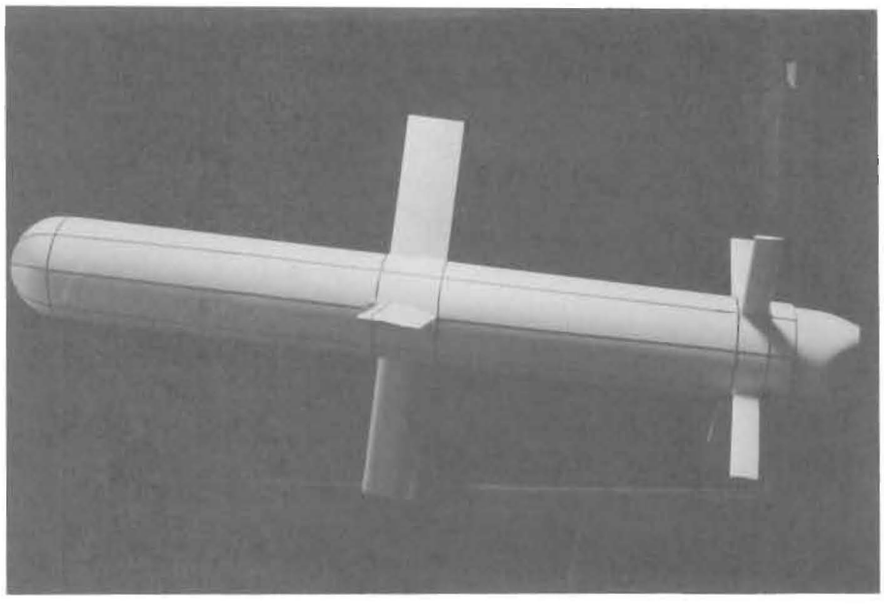

Figure 6. The one-third-scale TOW 2B missile model mounted in low speed wind tunnel .

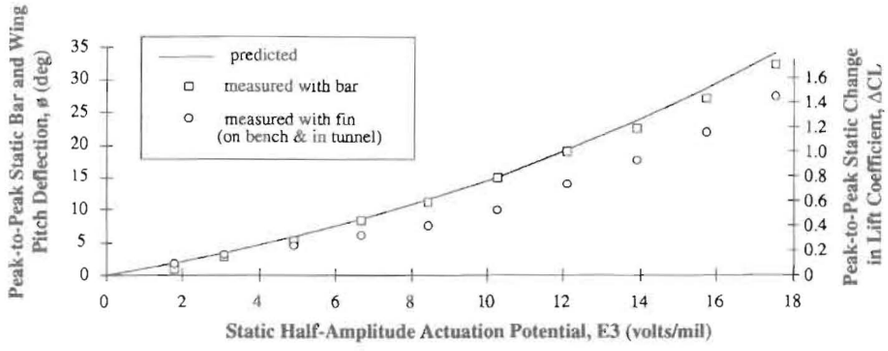

Figure 7. Pitch deflection and change in lift coefficient as a function of actuation potential.

3.2. Bender element testing

Experimental testing of the bender element was accomplished using laser-reflection techniques. The base of the bender was rigidly clamped, a mirror was mounted on the tip of the element and a laser was reflected off the mirror. The laser beam deflection was recorded and translated into an element curvature. Testing was conducted using a 0.5 Hz sine signal from 0 through ±90 V peak to peak (18 V mil^{-1}). No evidence of depoling, arcing or cracking was detected during testing. The data showed the characteristic second-order increase in deflection with voltage. Equation (3) was used to estimate the amount of curvature that the element experienced as shown in figure 3.

4. TOW missile model construction and testing

4.1. Scaled TOW missile model fabrication

A one-third-scale TOW 2B missile model was built from an aluminum fuselage with aluminum fins, polyester resin nose cone and graphite–epoxy wings. All components of the missile were scaled down in detail with the exception of the wings, which were built with a rectangular planform. (The actual TOW missile has rectangular planform wings with small triangles taken out of their trailing edges near the wing tips.) Figure 4 shows the geometry of the model.

The missile fuselage was constructed from 2 in diameter, 0.032 in 2024-T3 tubing with aluminum fins and graphite–epoxy wings. A polyester resin nose cone was machined to 2 in diameter. Accommodation for the adaptive wing was made by a 0.5 in long cutout in the center of the missile.

The scaled model was fitted with the adaptive wing which was built upon a graphite main spar and fiberglass root mount. The aerodynamic graphite shell was constructed from 25 mil thick bi-directional graphite–epoxy composite material. A brass end-plate was integrated onto the tip of the wing. Two holes in the end-plate were bored for accommodation of the end pivots. Internal and external leading-edge counterweights were used to mass balance the fin. Figure 5 shows the geometry of the wing, spar, shell and piezoceramic bender actuator.

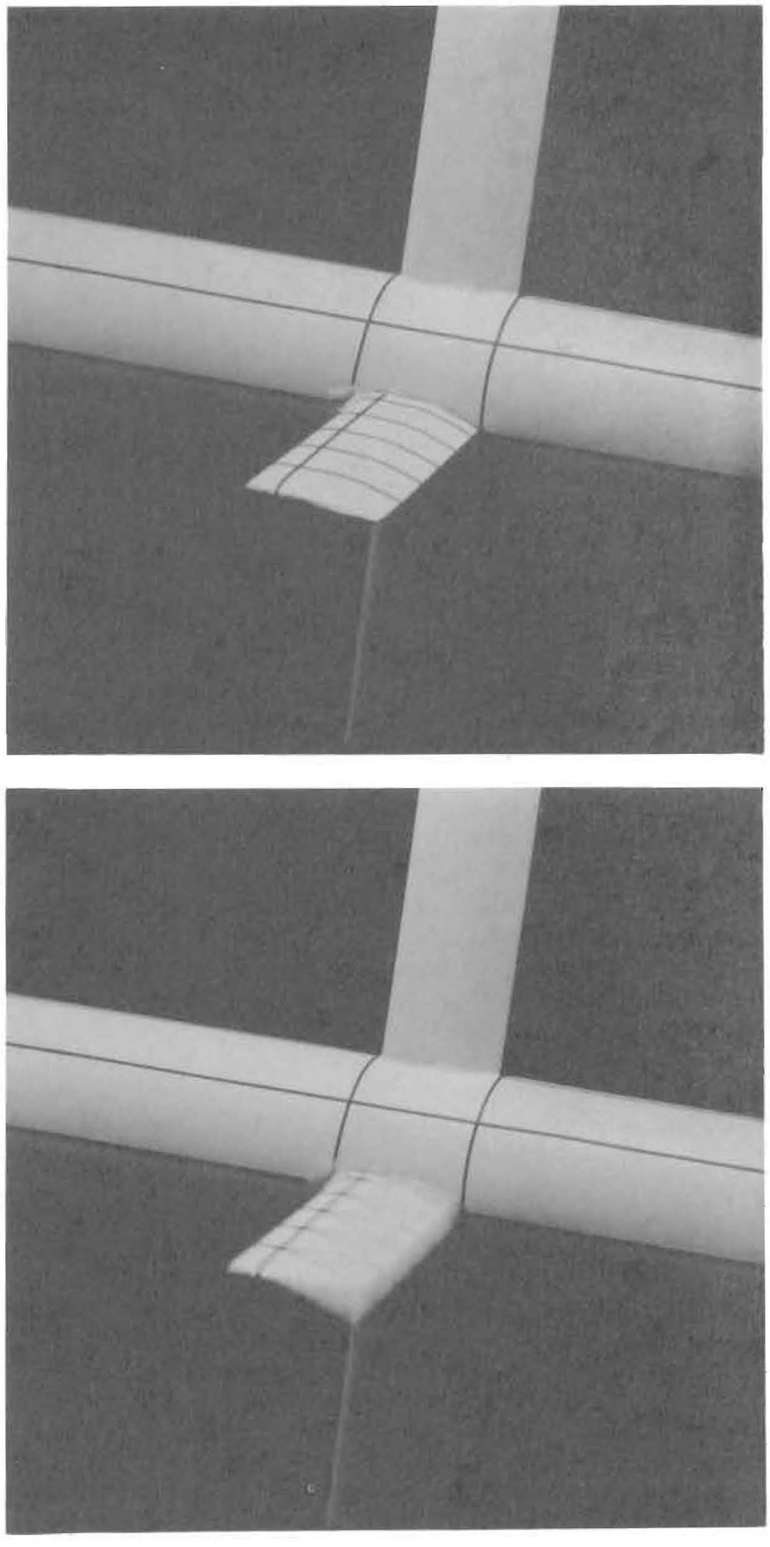

Figure 8. The static and dynamic flexspar missile wing at 12 Hz, ±8.1°, ±2 V mil^{-1} (±10 V AC).

4.2. TOW missile model and active wing testing

A series of tests were conducted on the missile model, active wing and actuator element. After mounting of the flexspar actuator, a pivot connection test bar was installed between the end pivots on the main spar and the bending actuator. A laser mirror was connected to the bar and the rotation of the bar was measured as a function of applied voltage as for element testing. The pivot connection bar was fitted with a loose tolerance of 1.5 mil to allow for free rotation without binding at high rotation angles. After using the test bar, the missile wing shell was mounted on the spar and the pitch deflections of the shell were measured as a function of applied voltage. One structural connection

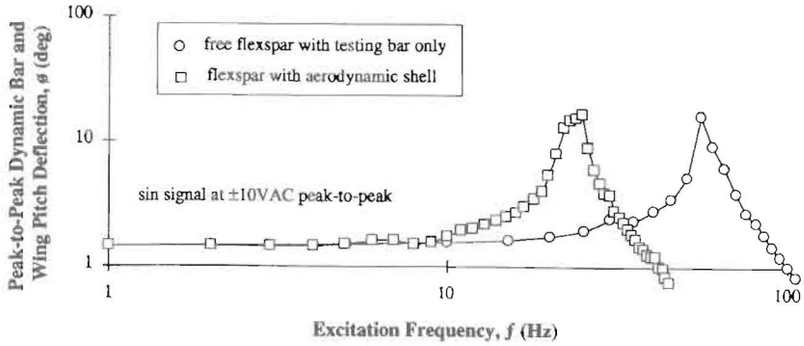

Figure 9. Dynamic characteristics of the flexspar actuator.

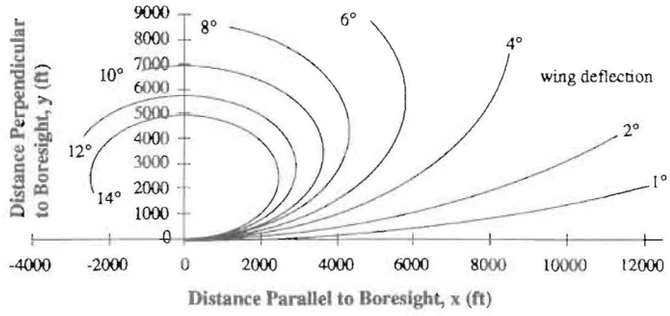

Figure 10. Minimum-radius turn flight profiles of a flexspar wing equipped TOW missile.

at the base and one at the tip of the main spar allowed the shell to rotate around the quarter-chord. The base pivot employed a 1/32 in steel pin which fitted within a brass root sleeve bearing. The tip pivots at the spar and the bender actuator also employed steel wires rotating within brass sleeve bearings.

Equations (3) and (5) were used to predict the pitch deflections of the bar and shell. From figure 1, the distances for the model were determined to be $l_0 = 2.1$ in, $l_{0_{tot}} = 2.4$ in and $l_1 = 0.4$ in. Additionally, the missile model was mounted on a sting and tested in the low-subsonic 1 ft × 1 ft wind tunnel at Auburn University. Changes in lift coefficient were measured along with wing pitch deflections. Figure 6 shows the configuration of the TOW missile model mounted on the sting in the wind tunnel. Figure 7 shows the variation in pitch angle and lift coefficient of the wing as a function of applied voltage.

The results of testing showed that deflections in excess of ±14° could be achieved and that the fin exhibited a lift-curve slope of $0.052^{\circ-1}$. Accordingly, the maximum change in lift coefficient was ±0.73. A series of dynamic actuation tests was also conducted on the missile model. Figure 8 shows the static and dynamic deflections of the missile wing in the wind tunnel. Dynamic testing was conducted with a ±10 V AC sine signal from 0.1 to 100 Hz with deflections measured, again, by laser reflection techniques. Testing with the pivot connection test bar was also conducted and showed that the natural frequency was 55 Hz with a break frequency of 107 Hz as seen in figure 9. With the shell attached, the natural frequency was reduced to 12 Hz with a break frequency of 25.5 Hz. Table 2 summarizes the test data, predictions and full-scale values. Power was measured by determining the applied voltage and current draw. Table 2 shows that the predicted values for pitch deflection are approximately 17% greater than the test values over most of the actuation range. It is thought that this disparity is caused by a small amount of friction in the hinges and slop in the end pivot connections. The resulting dead band due to this friction and slop was measured at approximately ±0.15°.

5. Missile flight performance improvement estimation

Because all flight control on current TOW missiles is carried out by only the aft fins, pitch deflections of the wings combined with the fins will bring significant improvements in maneuverability. Current literature indicates that the TOW 2B has a maximum effective range of 2.33 mi which is covered in 21 s after an initial launch velocity of approximately 1100 ft s^{-1}. A simple reverse engineering exercise considering a 2 s flight motor burn and small compressibility effects yields an estimate for the gliding flight profile. Assuming the flexspar wings are pitched to a maximum deflection for a minimum radius turn upon launch, the normal acceleration may be determined. If no body lift or lift from the fins is assumed, then a conservative approximation for acceleration as a function of wing pitch angle may be obtained. This estimation may be used to find the profile of the minimum-radius turn as a function of wing deflection as shown in figure 10.

6. Conclusions

This study has shown that laminated plate theory combined with kinematic models accurately predicts the amount of pitch deflection generated by flexspar actuators. These models and experimental testing also show that a one-third-scale TOW missile wing may be built with piezoceramic flexspar elements which drive the fins up to $\pm 14^{\circ}$ in pitch. Because these fins are both aerodynamically and mass balanced about the quarter-chord, they exhibit no tendency to diverge or flutter with changes in subsonic airspeed. Wind tunnel testing shows a $C_{L\alpha}$ of $0.052^{\circ-1}$ and a maximum change in lift coefficient of ± 0.73. An estimation of flight performance at maximum wing deflection shows that the minimum turn radius may be substantially reduced to less than 2400 ft.

Acknowledgments

The authors wish to acknowledge the Auburn University School of Engineering and Aerospace Engineering Department for supporting this research. The authors would also like to thank Dr Brian Chin and the Auburn University Materials Engineering Program for their consistent support, encouragement and assistance.

Nomenclature

A, B, D	extensional, coupling and bending stiffness matrices
C_L	lift coefficient
E_3	through thickness electric field
E_L, E_T	longitudinal and transverse element stiffness
N, M	applied forces and moments
t	thickness
ΔT	temperature change
T	thickness ratio $= t_s/t_a$
α	coefficient of thermal expansion angle of attack
ε	laminate strain
κ	laminate curvature
Λ	ith direction actuator free strains
ϕ	airfoil pitch angle

Subscripts

a	actuator
b	bond
s	substrate

References

[1] Crawley E F, Lazarus K B and Warkentin D J 1989 Embedded actuation and processing in intelligent materials *2nd Int. Workshop on Composite Materials and Structures (Troy, NY, 1989)*

[2] Spangler R L and Hall S R 1990 Piezoelectric actuators for helicopter rotor control *31st Structures, Structural Dynamics and Materials Conf. (Long Beach, CA, 1990.)*

[3] Hall S R and Prechtl E F 1994 Development of a piezoelectric servoflap for helicopter rotor control *31st Ann. Tech. Meeting Soc. Eng. Sci. (College Station, TX, 1994.)*

[4] Samak D K and Chopra I 1993 Feasibility study to build a smart rotor: trailing edge flap actuation *Proc. North Am. Conf. on Smart Materials and Structures (Albuquerque, NM, 1993)* pp 225–37

[5] Griffin S and Hanagud S V 1994 Smart aerodynamic control surface actuator *Proc. North Am. Conf. on Smart Materials and Structures (Orlando, FL, 1994)* pp 99–106

[6] Giurgiutiu V, Chaudhry Z and Rogers C 1994 Engineering feasibility of induced strain actuators for rotor blade active vibration control *Proc. North Am. Conf. on Smart Materials and Structures (Orlando, FL, 1994)* pp 107–22

[7] Barrett R 1992 Actuation strain decoupling through enhanced directional attachment in plates and aerodynamic surfaces *Proc. 1st Eur. Conf. on Smart Structures and Materials (Glasgow, 1992)* pp 383–6

[8] Barrett R 1992 Active plate and wing research using EDAP elements *J. Smart Mater. Struct.* **1** 214–26

[9] Barrett R M 1994 Active plate and missile wing development using DAP elements *AIAA J.* **32** 601–9

[10] Shiao M and Chamis C 1994 Optimization of adaptive intraply hybrid fiber composites with reliability considerations *Proc. North Am. Conf. on Smart Materials and Structures (Orlando, FL,)* pp 484–94

[11] Barrett R 1993 Aeroservoelastic DAP missile fin development *J. Smart Mater. Struct.* **2** 55–65

[12] Barrett R 1993 Modeling techniques and design principles of a low aspect ratio active aeroservoelastic wing *Proc. North Am. Conf. on Smart Materials and Structures (Albuquerque, NM)* pp 107–18

[13] Chen P and Chopra I 1993 Feasibility study to build a smart rotor: induced strain actuation of airfoil twist *North Am. Conf. on Smart Materials and Structures (Albuquerque, NM)*

[14] Barrett R 1993 Advanced low-cost smart missile fin technology evaluation *Final Report to the United States Air Force, Armament Directorate* contract No. FO8630-93-C-0039, Eglin A.F.B., Florida, Barrett Aerospace Technologies, Lawrence, KS

[15] Barrett R 1994 All-moving active aerodynamic surface research *31st Ann. Tech. Meeting Soc. Eng. Sci. (College Station, TX, 1994)*

[16] Barrett R 1994 A solid state apparatus for controlling pitch deflections of aerodynamic flight control surfaces *Auburn University Invention Disclosure* (patent pending).

[17] Jones R M 1975 Micromechanical behavior of a lamina *Mechanics of Composite Materials* (New York: Hemisphere Publishing)

[18] Anon 1990 *Piezo Systems Product Catalog* (Cambridge, MA: Piezo Systems)

[19] Anon 1992 *TOW 2B A Fly-Over Shoot-Down TOW* (Canoga Park, CA: Hughes Aircraft)